The influence of DC electric fields on small, laminar, premixed propane/air flames

Mário Pinto
mario.pinto@tecnico.ulisboa.pt

Instituto Superior Técnico, Universidade de Lisboa, Portugal

May 2018

Abstract

The present work evaluates the influence of electric fields in conical, laminar, premixed flames of propane/air, anchored in perforated plates. Ionic winds, caused by the interaction between the electric field and ions produced by the flame, modified the flow structure in two different modes. For characteristic burner exit flow velocities of 0.6 m/s and electric field strengths of 150 kV/m, it was verified a change in the flame appearance to a flattened form. This shape modification was caused by ionic winds which decelerated the flow above the flame. The flame deformation induced an increase of the average laminar flame speed (S_L^*) until 56%. With characteristic burner exit flow velocities greater than 1.0 m/s, maintaining the electric field, the flame reassumed the original conical form due to flow modifications promoted by the ionic wind in the flame anchoring region, measured in the literature. Consequently, S_L^* tended to the non-actuated value due to a reduction of flame stretch. In both cases, flame chemiluminescence demonstrated that these modifications do not affect the equivalence ratio (ϕ). However, the electric field promoted a flame stability increase, characterized by an expression which estimates the blow-off Re as a function of ϕ and electric field strength, E:

$$Re \cong m_0'(1+kE)\phi - m_0'(1+kE)LSL$$

where m_0' is the corrected slope of the blow-off line of the non-actuated flame, LSL is the lean stability limit and k is an experimental constant. This stability increase allowed a burner power density increase until 190% for $\phi = 0.8$.

Keywords: DC electric field, ionic wind, stability, chemiluminescence, PIV, laminar flame speed.

1. Introduction

Combustion is broadly diffused in modern societies. This generalized usee amplified the emissions and energy sustainability problems. These problems forced combustion to be performed in lean conditions to reduce emissions although the problem is not fully resolved and on other hand, new issues related with stability appear. Therefore, combustion research has the responsibility to confront these issues.

In addition, industry is now focusing on miniaturization combustion systems involving laminar, premixed flames to reach portable dimensions. As a consequence, the burner hole size is being reduced and the number of holes is increasing to create multiperforated surfaces, able to withstand smaller, independent flames. With this type of systems, new problems arise mainly due to heat losses to the wall and blow-off which hinder the flame's control and stability. These new difficulties triggered a quest for alternatives to aid miniaturized combustion systems. One new concept with possibilities to enhance the stability of flames involved in these systems is electric field assisted combustion.

Flames are chemical reactions with complex kinetical mechanisms which involve several species. While the majority of these species is electrically neutral, some have a non-neutral electric potential, named charged particles, and are balanced in two major groups, positive and negative. While the positive ones are composed only by positive ions, the negative ones are composed by free electrons and negative ions.

Important positive ions in hydrocarbon flames feature H_3O^+, CHO^+, $C_3H_3^+$, $C_2H_3O^+$ and CH_3O^+ [1]. For negative charged particles, some negative ion production exists, but ultimately, the key role can be attributed to free electrons [2].

Charged species are formed by ionization and destroyed by recombination. According to Fialkov [2], ionization reactions, typically occur in or nearby the flame front, and recombination reactions arise in the combustion products region.

The concentration of charged species is conditioned by the temperature gradient and the local equivalence ratio,ϕ. In a Bunsen flame at atmospheric pressure, this originates a complex distribution of charged

species, specially near the burner rim, where the flame front is enclosed by cold gas with species extremely reactive with free electrons [2].

The presence of charged particles make flames sensitive to external electric fields applied. In addition, the characteristics of the electric fields applied are determinant factors in the flames' response.

For the case of a Direct Current (DC) electric field applied to a flame, a possible configuration features a metallic mesh and a burner plate which are used to apply a voltage, ΔV. If the electric perturbations induced by the flame's charged particles are not accounted and the distances between electrodes, h, are small enough ($\sim 1cm$), a uniform electric field approximation is allowed. In this case, the electric field strength, E, is calculated with equation 1.

$$E = \frac{\Delta V}{h} \tag{1}$$

When a flame is under the effect of an electric field, charged particles are accelerated by the Lorentz force [1]. Charged particles eventually collide with neutral ones and the momentum transfer during collisions induces a bulk flow motion, known as ionic wind [2, 1]. Other mechanisms feature the modification of transport properties of charged species [3] and changes in the chemical kinetics gained via kinetic energy of accelerated charged species [4]. For the case of laminar, premixed, conical flames, a separation of effects is complicated.

Electrical properties of flames can be used to model combustion conditions, by applying an electric field sufficiently strong to obtain the desired effects. The main findings feature increases in propagation velocity [5, 6], laminar flame speed [4, 3, 7] and combustion rate [8]. Stability gains in the blow-off limit were also described as dependent on field polarity [9]. Flow modifications were also observed by using Particle Image Velocimetry (PIV) with the scope of characterizing the effects of the ionic wind in the flow field [10, 11, 12, 13], with 6 to 16kV applied, but also considerable electrode distances $h \approx 50$ mm. Effects on pollutants and emissions were also registred [14, 15], mainly in CO and NO_x. Flame acoustics was also adressed with discoveries in control [16] and reduction of instabilities [17]. CH^* [18] and OH^* [19] chemiluminescence provided important information connecting the observed effects to the kinetic mechanisms behind ionization/recombination reactions in nonpremixed flames.

Regarding works with premixed flames, two main case studies appear in the literature: conical and flat. Important characteristics of these studies, related with electric field (electrode distance, applied voltage, electric field strength) and geometry (burner diameter) are compared in Figure 1 with the ones from the present work. Flat flames enable lower electrode distances ($h \approx 10$ mm) due to their lower flame height with respect to conical ones. As a consequence, strong electric fields can be obtained with the same (or even lower) voltages applied. However, this advantage can also be explored in conical flames if its dimensions allow it, which is higly convenient for miniaturized and portable combustion systems.

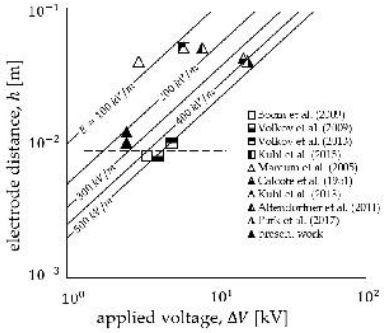

(a) Electrode distance and applied voltage.

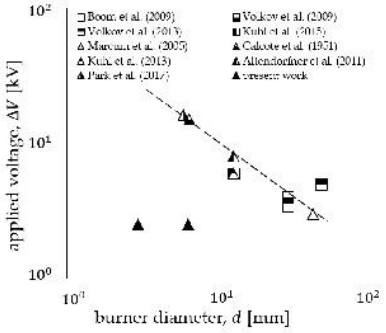

(b) Applied voltage and burner diameter.

Figure 1: Experimental parameters used in works with DC electric fields.
□ – flat flames; △ – conical flames.

The objective of the present study is to investigate the influence of a DC electric field in small (3 to 6.5 mm diameter), laminar, premixed propane-air flames, as mapped in Figure 1. Subsequently, the stability, morphological and flow responses of flames to DC electric fields will be described. Estimates on the average laminar flame speed modifications will be reported in this work.

2. Experimental set-up

The core structure for this work features the burner and electric field equipment, to which are added other devices necessary to perform the experimental work. An aluminium, 380 mm long divergent-convergent nozzle burner structure was used. A propane (C_3H_8) and dry air mixture enters at the bottom of the burner through two flow inlets and exits at the top where one disk shaped burner plate is bolted.

Two plates, A and B (Figure 2), were tested. Plate A was used for stability, morphology and spectroscopic

analysis while Plate B was used for stability, morphology and PIV analysis. A circular (100 mm diameter), made of steel wire, squared mesh (1.5 mm side, 0.5 mm wire thickness) electrode was mounted above the burner at an adjustable height. To provide the electric field, a DC power supply applied a potential difference between the electrode and the grounded burner.

Figure 2: Plate A (d=3 mm) and Plate B (d=6.5 mm).

The complete experimental setup utilized is represented in Figure 3. It features the necessary equipment to control and visualize the flame and also to perform emission spectroscopy and PIV.

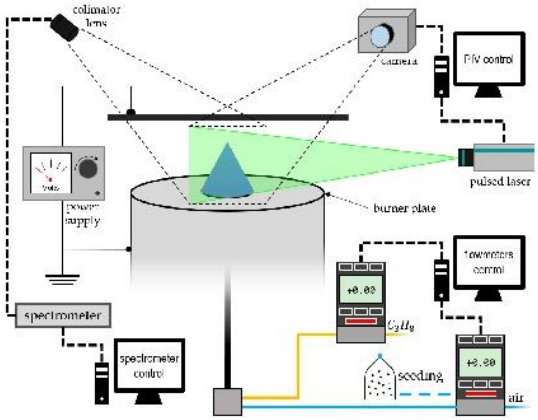

Figure 3: Scheme of the experimental setup.

To regulate the flow and premixture conditions two digital flow meters (Alicat Scientific MC-1SLPM-D/5M for propane and MC-5SLPM-D for dry air) controlled by a LabVIEW developed application, were used. Two camera setups, were used given their complementary characteristics. The Canon EOS-7D with an EF-S 18-135mm f/3.5-5.6 IS lens set up used on an initial approach due to its practical characteristics. For an enhanced view of the flame front, the Zyla 5.5 sCMOS along with an AF Micro NIKKOR 60mm F2.8D lens with a CH^* filter. ImageJ was used to analyse the pictures and extract measurements.

To perform emission spectroscopy it was used an Ocean Optics' HR4000 spectrometer and an optical fibre. To avoid divergence of the scope area, a collimator lens was mounted on the tip of the optical fibre. For each test, 50 spectra were collected to assure a statistically strong result and the integration time was set to 1 second. MATLAB routines were used to process the spectra. The program sequence performed background subtraction, built the spectra graphics, obtained the peaks of OH^*, CH^* and C_2^* radicals and computed the peak ratios: OH^*/CH^*, CH^*/C_2^*, C_2^*/OH^* for each test.

PIV equipment featured a Dantec Dual Power 65-15 Yag laser, with two laser cavities and a maximum frequency pulse of 15 Hz, produced a light sheet ($l_s \approx 1$ mm). To capture the necessary frames the Zyla 5.5 sCMOS along with an AF Micro NIKKOR 60 mm F2.8D lens camera setup with a band pass filter that centred at 532 nm. The laser and the camera were both connected to a Dantec FLOWHUB 1500 hub which was connected to a workstation computer. Due to statistical reasons, the number of collected images per run was set to 150. The acquisition mode was set to double frame, meaning two consecutive frames per image were collected in an interval of 40 μs. For post-processing each test, a cross-correlation method was conducted for each image with an interrogation area of 64×64 pixels with an overlap of 50% on both directions. After this, a range validation based on the velocity magnitude was performed. Then, the 150 vector maps were averaged into one. The Seeding particles used for the PIV tests were Aluminium Oxide, Al_2O_3.

3. Results

3.1. Flame Stability

With the purpose of evaluating the effect of the electric field on the stability of laminar, premixed propane/air flames, the blow-off stability limit was quantified. Stability charts were made using the equivalence ratio and Reynolds number as parts of a coordinate system(ϕ, Re). The results are displayed in Figure 4, where the blow-off Re is illustrated as a function ϕ for different values of E and for both plates. It is noticeable a linear increase in the blow-off Re with the increase of ϕ. This can be explained by the blow-off gradient behaviour and exterior air diffusion into the mixture which increases the local flame speed near the burner rim (the flame's anchoring point) for fuel-rich mixtures.

This tendency was maintained as the electric field strength increased. Furthermore, the linear characteristics of this increase made possible to perform a linear regression to every set of points collected from each test and associate a slope, m, and the y-interception, b. The obtained expression is provided by equation 2. Under this line the flame is considered to be stable and above this line the flame can no longer stabilize itself and extinquishes.

$$Re = m\phi + b \tag{2}$$

By setting $Re = 0$ and solving equation 2 to find the corresponding equivalence ratio, the lean stability limit, $LSL = -b/m$, is obtained.

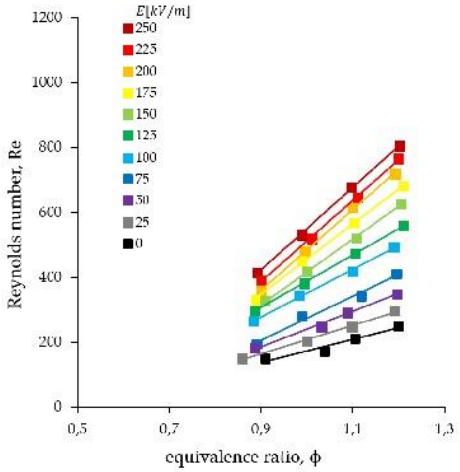

(a) Plate A, $d = 3$ mm

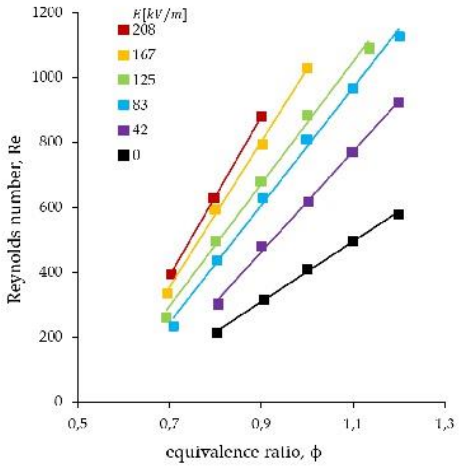

(b) Plate B, $d = 6.5$ mm

Figure 4: Stability Diagrams.

It is concluded, for these conditions, that the electric field does not alter the lower stability limit since the experimental values do not diverge from an average value of $\phi = 0.558$. This implies that all lines must pass in this point and consequently, the y axis interception is a projection of the line passing through the lean stability limit and its value is controlled by the slope.

Accordingly, a new variable X^*, was created as a subtraction of LSL to ϕ and is defined by $X^* = \phi - LSL$. In Figure 5 is represented the blow-off Re as a function of X^* instead of ϕ, for different values of E. New lines were traced for each test and were forced to pass in the origin of the referential, which is now LSL. With this, the y axis interception was fixed at $b = 0$ and new corrected values for the slopes, m', were obtained. The blow-off lines are now $Re = m'X^*$.

The slope of the lines increases with applied electric field for both plates, yet a possbile relationship between

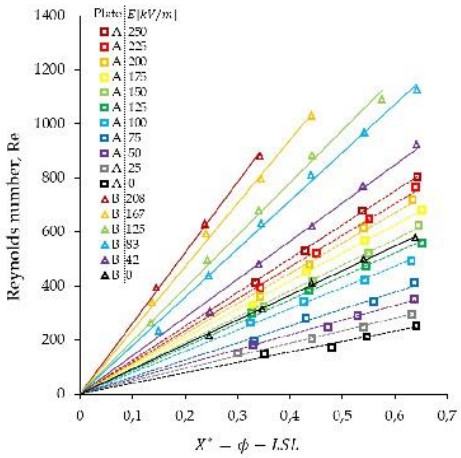

Figure 5: Modified stability diagram: Re *vs.* X^*.

the electric field and the slope is still unclear in a way that the lines obtained for Plate A are not relatable to the ones for Plate B. To resolve this, the values for the corrected slopes with no electric field applied, m'_0, can be described as a derivative: $m'_0 = \frac{\partial Re}{\partial \phi}$. After expanding and analysing the terms' orders of magnitude, the result in equation 3 was obtained, where $\frac{\partial V'_0}{\partial \phi}$ is the velocity gradient with the equivalence ratio.

$$m'_0 \cong \frac{d\rho}{\mu} \frac{\partial V'_0}{\partial \phi} \tag{3}$$

To verify this solution, new m'_0 values obtained with equation 3 for both plates were compared with the corresponding experimental ones. Since deviations were not significant (under 10%) the dominant effects in m'_0 are: burner diameter (d), a direct geometric parameter, and the velocity gradient with the equivalence ratio $\left(\frac{\partial V'_0}{\partial \phi}\right)$, which is also influenced by geometry.

The experimental values for m'_0 were taken as references for each plate, and the normalised slope, $\bar{m}$, was defined as $\bar{m} = (m' - m'_0)/m'_0$. In Figure 6 is displayed the proportionality relationship between the E and the experimental values of $\bar{m}$. A proportionality constant, k, was obtained regarding all points.

The resulting equation 4 relates the normalized slope as a function of the applied electric field made possible by the finding of constant k.

$$\bar{m} = kE \tag{4}$$

By expanding the first member of equation 4 using the definition of $\bar{m}$ and rearranging the terms, equation 5 exposes the corrected slope, m', as a function of the corrected slope without an electric field applied, m'_0, and E.

$$m' = m'_0(1 + kE) \tag{5}$$

Returning the analysis to Figure 5, m' is the only parameter influencing the differences between the blow-off lines. A new variable Y^*, was defined as $Y^* =$

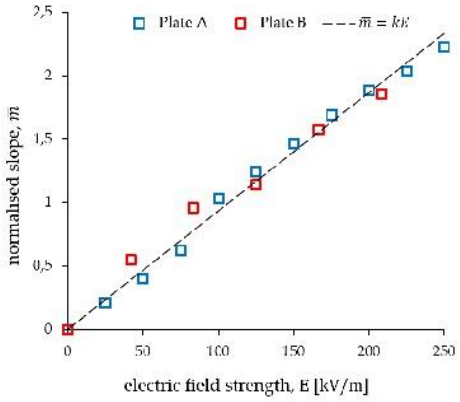

Figure 6: Linear behaviour of $\bar{m}$ with respect to E

Re/m'. Replacing m' with the second member of equation 5, it is possible to relate directly the blow-off Reynolds number with E. The result of this combination is equation 6.

$$Y^* = \frac{Re}{m'_0(1+kE)} \tag{6}$$

A new stability diagram was obtained by transforming the initial blow-off coordinates (ϕ, Re) into (X^*, Y^*). The transformed points are represented in Figure 7 and are spread along the line $Y^* = X^*$, which represents the normalized blow-off line, above which the flame extinguishes and under which the flame can be stabilized.

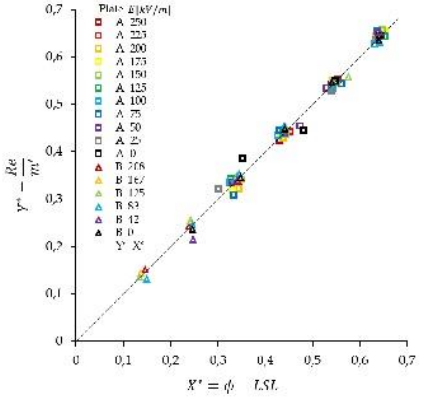

Figure 7: Modified stability diagram: Y^* *vs.* X^*.

By expanding $Y^* = X^*$, all variables are exposed in equation 7, which expresses the blow-off Reynolds number (flow conditions), as a function of the mixture conditions (equivalence ratio and lower stability limit), geometry (corrected velocity gradient with the equivalence ratio with no electric field applied) and the electric field. It is concluded that the normal blow-off conditions are improved by a factor of $(1 + kE)$. Furthermore, within the ranges tested, equation 7 successfully estimates the blow-off Re at given ϕ and E conditions based only on the blow-off line at $E = 0$.

$$Re \cong \frac{d\rho}{\mu}\frac{\partial V'_0}{\partial \phi}(1+kE)\phi - LSL\frac{d\rho}{\mu}\frac{\partial V'_0}{\partial \phi}(1+kE) \tag{7}$$

Additionally, the stability increases reported allow more propane to be burned, maintaining the equivalence ratio. Consequently, flame power is also increased. When this power is divided by the area of the burner hole, the power density of the burner is obtained. As it is an important burner design parameter, calculations were made with the stability diagrams of both plates, to perceive the impact of E in burner performance. The results for $\phi = 0.8$ and $\phi = 0.9$, have particular relevance since they describe the complete evolution and the flame is in lean conditions. For these two cases, the increases in power density reach 190% and 178%, respectively for Plate B and 173% at $\phi = 0.9$ for Plate A. Furthermore, the maximum power density achieved with the applied electric field can match or surpass the power densities at $E = 0$ of stoichiometric and slightly rich flames. Therefore it is concluded that E has a beneficial impact in burner performance.

3.2. Flame Morphology

In Figure 8 is displayed a series of images collected with CH^* filter. These images depict the evolution of different flames as E is increased. The equivalence ratio ranged from $0.9 < \phi < 1.2$ and the Reynolds number was fixed at $Re = 260$ and $Re = 290$. On a first observation, it is evident the flattening of the flame profile as E increases.

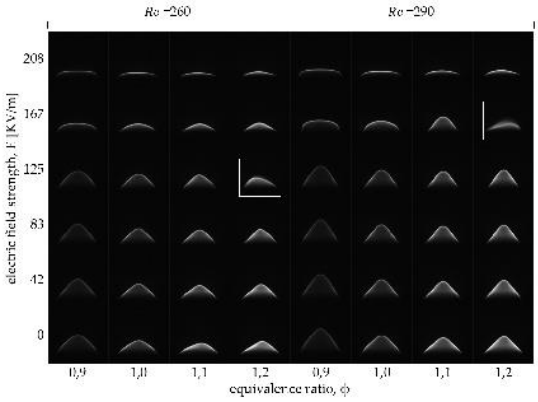

Figure 8: General flame appearance modifications with E observed with Plate B. White squares highlight images captured in the transition regime.

The electric field forced the flame tip to flatten with higher electric field strengths (167 kV/m and 208 kV/m) after reduced modifications, in the inferior range of electric fields applied (42, 83 and 125 kV/m). These reduced modifications at low values of E are difficult to be perceived on an initial approach

as the flame preserves its normal, conical shape. A third type of flame shape appeared, characterized by an oscillatory behaviour, in the transition between the two shapes previously mentioned, with a frequency on the order of 10^1 Hz. Although acknowledged, further information on this type of flames was not collected.

Focusing the analysis on the images with $\phi = 1.1$ and $E = 167$ kV/m, at $Re = 260$ and $Re = 290$, the flame returns to its original shape once Re was increased. This finding displays Re as a determinant factor in the shape change. With a sufficient increase of Re, the flame with the electric field applied returns to its original conical appearance. In fact the values of Re to collect these images were chosen with the intention of observing this shape change.

It is important to note that flame shape modifications are deeply dependent on experimental conditions, mainly: fuel, type of flame and E. Kuhl *et al.* [10], for example, observed no visible changes with a conical methane/air flame and $E = 120$kV/m, for stoichiometric conditions with an average flow velocity at the burner exit of 2.0 m/s. However, Marcum *et al.* [3] noted a wrinkled geometry with signs of turbulent flow similar to the transition region highlighted in Figure 8 with a propane/air flame and $E = 75$ kV/m at $\phi = 1.2$ and an average flow velocity at the burner exit of 1.2 m/s.

3.3. Flattened flame characterization

In this section the flatenned flame, previously approached in section 3.2, is further explored and compared with its original conical form at $E = 0$, through series of tests in this scope. The presented results offer insights in flame chemiluminescence, flow structure to explore chemical effects and ionic wind, respectively and how these modifications are reflected in a key combustion parameter, the laminar flame speed, S_L.

3.3.1 Flame Chemiluminescence

Emission spectroscopy testes were performed with Plate A. The flame conditions for these tests featured a fixed $Re = 180$ and $0.85 < \phi < 1.20$. The spectra were obtained with an electrode distance of 10 mm and with an applied voltage of 2500 V, equalling an electric field strength of 250 kV/m sufficiently high to flatten all flames.

An example of the obtained spectra is available in Figure 9, which compares two spectra at $Re = 180$ and $\phi = 1.15$, one with $E = 0$ (blue line) and another one with $E = 250$ kV/m (black line). As Figure 9 depicts, all points of the spectrum appear to increase proportionally, due to an increase of flame luminosity by the electric field. Therefore, once applied, the electric field did not affect the general flame colour, only intensity.

For a detailed evaluation of the global differences between the spectra, chemiluminescence ratios based

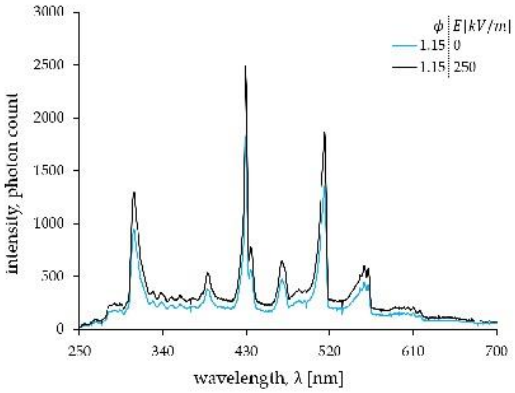

Figure 9: Emission Spectra
Plate A, $Re = 180$, $\phi = 1.15$.

on radical peak intensity were calculated and compared with values obtained by Trindade [20]. The obtained results for the variation of peak intensity ratios with ϕ at $E = 0$ and $E = 250$ kV/m are displayed in Figure 10.

For results with $E = 0$ there is a tendency agreement with Trindade [20], as the experimental values follow the same evolution. For OH^*/CH^* ratio, due to interference of the flame plume, which emits CH^* but mostly OH^* and almost no C_2^* there is a minor deviation in the values obtained. This interference is larger in the flame of Trindade [20] ($d = 20$mm) as the flame tested in the present work is smaller ($d = 3$mm) and thus, the plume is less intrusive.

Once the electric field was applied, the points continued to follow the same trends for all chemiluminescence ratios in Figure 10. This finding suggests that any significant variations occurred in chemical kinetics do not change the ratios between excited radicals. This result implies that the equivalence ratio detection by chemiluminescence is not altered by the electric field, as all radicals increase the corresponding peak intensities proportionally.

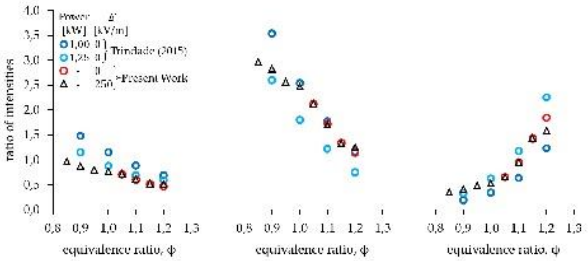

(a) OH^*/CH^* (b) CH^*/C_2^* (c) C_2^*/OH^*

Figure 10: Variation of peak intensity ratios with ϕ at $E = 0$ and $E = 250$ kV/m. Plate A, $Re = 180$. ◯ – $E = 0$; △ – $E = 250$ kV/m.

3.3.2 Flow Modifications

To investigate the influence of the ion driven wind caused by the electric field, a flow evaluation was performed through the use of the particle image velocimetry (PIV) technique. Plate B was chosen for these tests since it allowed to stabilize flames at higher flow rates which are capable of transporting more seeding particles. The Reynolds number was fixed to 290 corresponding to a flow velocity of 0.685 m/s sufficient to observe the flame flattening with an electric field applied.

In Figure 11 are displayed two half flames and its corresponding velocity vector maps with the same mixture settings ($Re = 290$, $\phi = 1.2$) as an example. The flame on the left side has $E = 0$ and the one on the right side has $E = 212$ kV/m.

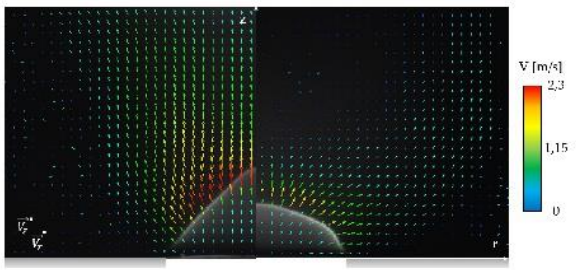

Figure 11: Velocity map for flames with and without electric field applied. Left side: $E = 0$. Right side $E > 0$. Plate B, $Re = 290$, $\phi = 1.2$, $E = 212$kV/m.

To further explore the differences caused by the electric field, velocity maps of flames with $E = 0$ were subtracted to velocity maps of flames with the same mixture conditions (Re, ϕ) with an electric field applied ($\vec{V}_{E>0} - \vec{V}_{E=0}$). One example is displayed in Figure 12 which illustrates the resulting vector map obtained with the two velocity vector maps with $Re = 290$ and $\phi = 1.2$ (previously displayed in Figure 11).

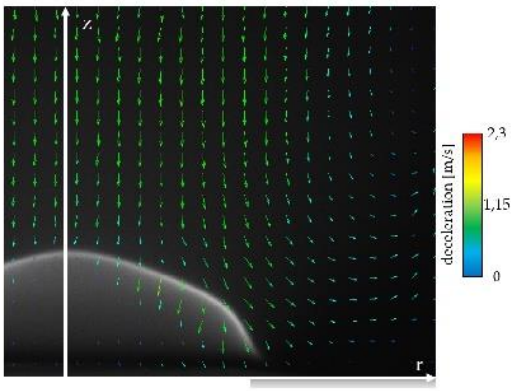

Figure 12: Detailed view of the flow deceleration caused by the electric field. Obtained with $\vec{V}_{E>0} - \vec{V}_{E=0}$. Plate B, $Re = 290$, $\phi = 1.2$, $E = 212$ kV/m.

This result further illustrates the modifications caused by the electric field. The ion wind caused by the electric field, creates a flow deceleration (≈ 1.1 m/s), mostly in the region above the flame, coincident with the direction of the electric field. This vertical deceleration causes the flow to deviate to the sides of the flame, modifying the flow in the flame anchoring region (≈ 0.8 m/s).

The flow deceleration also indicates that the dominant component of the ion wind is induced by positively charged particles, which are accelerated towards the burner, contrary to the flow. The region where this effect assumes larger magnitudes is along the central axis of the conical flame, z (where $r = 0$), coincident with the direction of the ionic wind.

Kuhl *et al.* [12] also observed flow decelerations while studying methane/air premixed flames at an average velocity at the burner exit of 2.0 m/s. However, since the flame was able to maintain its conical shape with $E = 120kV/m$, the region where larger modifications were observed was near the burner rim (flame anchoring region).

In the present work, despite the flame anchoring region being also affected, the principal differences appear in the central axis, as a flow stagnation zone appears above the flame on the right half of Figure 11 (where $E = 212$ kV/m).

3.3.3 Laminar Flame Speed

The electric field is capable of changing the visual aspect of flames due to modifications in the velocity field caused by ionic wind. This result suggested laminar flame speed modifications. To obtain experimental results for the laminar flame speed, a compatible method to measure it must be adopted.

One solution is to approach the mass conservation between the burner exit and the section immediately before the flame front, where the mixture is still cold and no reaction has occurred. With these boundaries, the average laminar flame speed, S_L^*, becomes dependent only of burner area, A_b, flame area, A_f and the velocity of the reactants, as described in equation 8.

$$S_L^* = V\frac{A_b}{A_f} \tag{8}$$

Regarding the terms of equation 8, the flame area is the one which can not be determinated with ease, as results depend on the optical method/criterium defined. One method available is photography which captures the luminous zone slightly after the reaction zone, where the temperature reaches its maximum value.

This method has coarse precision but was chosen due to its simplicity. To improve precision a CH^* band pass filter was placed in front of the camera to have a clear image of the reaction zone. Considering this, the images collected with the CH^* band pass filter previously

presented in Figure 8 were further used to estimate the flame area. Given the axisymmetric characteristics of the flame regardless of its shape, the flame surface can be approximated by a number of bands, formed by lines which rotate about the z axis. Each band has length l_i and an average radius relative to the z axis, r_i. The area of the approximated surface is calculated with the sum of all bands as displayed in equation 9.

$$A_f \cong \sum_{i=1}^{n} 2\pi r_i l_i \tag{9}$$

However, the z axis position in the image is difficult to define graphically, which inserts a source of error to the calculation. To minimize this, new quantities, directly measurable in the image were used. These are the total length of the flame front in the image, L_f, and the flame width, w_f. To fit in the equation 9, the two measured parameters were halved since only half of the flame is rotated around z. Furthermore, the value of the radius which fits the equation 9 is an average radius, therefore, the flame width was halved again. The adjusted equation 10 estimates the flame area directly from the parameters measured with ImageJ software. Finally, the average laminar flame speed was estimated directly from the application's outputs with equation 11.

$$A_f \cong 2\pi \frac{1}{4} w_f \frac{1}{2} L_f = \frac{\pi}{4} w_f L_f \tag{10}$$

$$S_L^* \cong \frac{\frac{\pi}{4} d^2}{\frac{\pi}{4} w_f L_f} V = \frac{d^2 V}{w_f L_f} \tag{11}$$

Equation 11 enabled the extension of the calculations to flames with an electric field applied. The electric field promotes an increase of the laminar flame speed until a saturation point is reached at higher values of E, as presented in Figure 13. Additionally, as the mixture becomes richer, the S_L increase is greater, the saturation region is also delayed. The maximum increase in S_L obtained was 56%.

3.4. Flame evolution towards high Reynolds numbers

It was demonstrated that the electric field increased the stability. The blow-off Re increased for all ϕ and E tested. This behaviour implies more pronounced improvements in rich flames ($\phi > 1$) than in lean flames ($\phi < 1$), with a linear variation regarding ϕ.

During the flame stability tests, flattened flames were observed. These were described as a result of ideal conditions between E, Re and ϕ. Chemiluminescence results suggested a possible influence of the electric field in chemical kinetics, whithout altering the equivalence ratio. On other hand, in the flow structure, the ionic wind was observed. Important flow modifications were visualized with PIV, in particular for rich mixtures. This modifications were characterized by a general flow deceleration in the region above the flame,

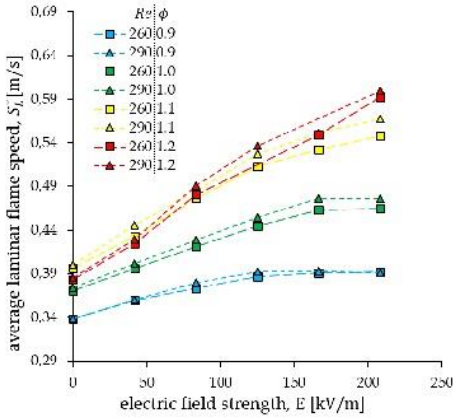

Figure 13: Laminar flame speed as E is increased. Values obtained from the images from Figure 8. Plate B. $\square$ – $Re = 260$; $\triangle$ – $Re = 290$.

which explained the flattened shape. This deceleration caused a deviation of the flow to the sides, accelerating the flow near the burner rim. In addition, estimates on the average laminar flame speed were performed as the flame evolved to the flattened form. It was observed an increase of S_L^* with E, caused by the flame curvature stretch induced by the ionic wind. This modification was more pronounced in rich flames (56% at $\phi = 1.2$) than in lean flames (16% at $\phi = 0.9$).

This section acesses the evolution of the flame under the effect of the electric field as Re is increased towards blow-off. In Figure 14 is presented a sequence of images of a flame with $\phi = 1.2$ under a constant $E = 208$ kV/m, as Re is increased, towards blow-off. It is noticeable that, as Re increases, the flame reassumes a conical shape (from $Re = 250$ to $Re = 350$). After this, the flame retains this shape and the flame height starts increasing with Re.

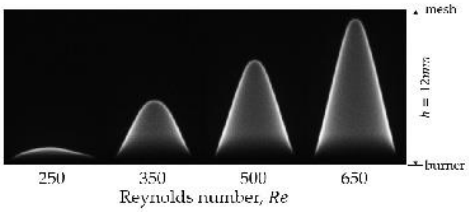

Figure 14: Sequence of flame images as Re is increased at constant $E = 208$ kV/m. Plate B, $\phi = 1.2$.

The images in Figure 14 were further used to estimate S_L^* as Re increases. The result is depicted in Figure 15, which displays the evolution of the average laminar flame speed of a flame with $\phi = 1.2$ under a constant $E = 208$ kV/m, as Re is increased, towards blow-off. It is demonstrated that once the flame becomes conical, S_L^* tends towards the original value at

$E = 0$ (0.38 m/s). This is due to the reduction of curvature induced flame stretch, which affects the laminar flame speed [23].

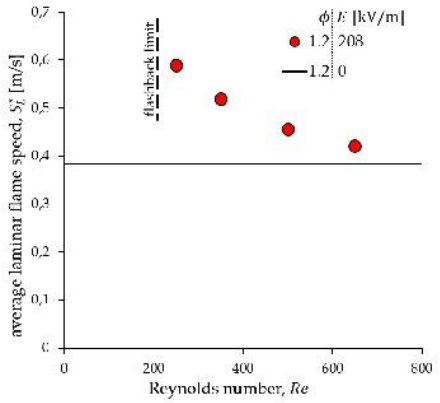

Figure 15: Evolution of S_L with as Re is increased at constant $E = 208$kV/m. Plate B, $\phi = 1.2$.

In addition, the velocity modifications induced by the ionic wind tend to decrease once the flame becomes conical, in particular, the flow deceleration in the region above the flame. However, these modifications can still be present since the only conditions required are the existance of charged particles and the electric field.

Kuhl *et al.* [12] studied the velocity modifications of laminar, premixed, conical methane/air flames under the effects of DC electric fields. For conical flames at $E = 120$ kV/m and at a constant exit flow velocity of 2.0 m/s, Kuhl *et al.* [12] observed maximum flow deceleration values in the flame anchoring region of 1.6 m/s at $\phi = 1.25$, 1.2 m/s at $\phi = 1$ and 0.8 m/s at $\phi = 0.83$. These values present an increase of the maximum flow deceleration with ϕ, consistent with the increase of the blow-off Reynolds number with ϕ. In addition, flow deceleration also increases with the electric field strength, which is also consistent with the trends observed in the flame stability analysis.

Since the flame anchoring region has an important role in blow-off control [24, 25], causes of the stability increase previously reported can be related to modifications in the flame anchoring region caused by the electric field.

Therefore, it can be concluded that the cause of the stability increase are flow modifications due to ionic wind near the flame anchor region. This conclusion is sustained on the evolution from the flattened flame to the conical form. This evolution is characterized by the reduction of the laminar flame speed towards blow-off and by the flow modifications caused by the electric field once the flame becomes conical, reported by Kuhl *et al.* [12].

4. Conclusions

In this work, the effects of high voltage DC electric fields on laminar, premixed, conical flames were experimentally examined. The principal conclusions are hereby numbered:

1. A stability increase was obtained with both plates. The slope, m increased with E and, once normalized ($\overline{m}$), was found to be directly proportional, with $k = 9.32361 \times 10^{-3}$ m/kV.

2. An alternative coordinate system (X^*,Y^*) was conceived which reavealed an expression of the blow-off limit, generalized for burners with small diameters (in equation 7). It was concluded that blow-off is dependent on mixture and geometry conditions, amplified by kE.

3. Flame imaging captured two core behaviours observed: conical and flattened.

This flattened shape of the flame motivated further analysis of the phenomena with the study of flame chemiluminescence and flow structure. In addition, estimates on the average laminar flame speed were also performed.

4. Flame chemiluminescence revealed an increase in the measured intensity with E. Furthermore, peak intensity ratios suggested that any modifications in the chemical kinetics do not alter equivalence ratio detection by chemiluminescence.

5. PIV tests displayed generalized flow modifications which explained the changes in the flame shape.

6. Estimates for S_L^* were computed, based on mass flow conservation. After necessary approximations, equation 11 was obtained. Results revealed an increase in S_L^* (with a maximum of 56%), more evident as E increases and for richer mixtures. This increase was consistent with the flame aspect modifications previously reported in section 3.2, which displayed increased flame curvature stretch and explained the estimated values.

However, as Re is increased towards blow-off, the flame reassumed the conical shape and S_L^* tended towards the original value at $E = 0$ due to a reduction of curvature stretch. Moreover, flow modifications in the region above the flame decreased as the flame became conical, despite ionic wind still being present. Accordingly, local flow modifications due to ionic wind near the flame anchoring region are proposed as the cause of the stability increase. These flow modifications, caused by ionic winds, on conical flames near the flame anchoring region were previously observed by Kuhl et al. [12].

5. Acknowledgements

The author would like to profoundly thank Professor Edgar Fernandes for all the supervision and guidance along all the stages of this work.

References

[1] James Lawton and FJ Weinberg. Electrical aspects of combustion, 1969. *London: Clarendon P. ISBN: 0-19-855341-2*, 1970.

[2] Alexander B Fialkov. Investigations on ions in flames. *Progress in Energy and Combustion Science*, 23(5-6):399–528, 1997.

[3] SD Marcum and BN Ganguly. Electric-field-induced flame speed modification. *Combustion and Flame*, 143(1-2):27–36, 2005.

[4] JDBJ Van Den Boom, A Alexander Konnov, AMHH Verhasselt, VN Kornilov, LPH De Goey, and Henk Nijmeijer. The effect of a dc electric field on the laminar burning velocity of premixed methane/air flames. *Proceedings of the Combustion Institute*, 32(1):1237–1244, 2009.

[5] HC Jaggers and A Von Engel. The effect of electric fields on the burning velocity of various flames. *Combustion and Flame*, 16(3):275–285, 1971.

[6] SH Won, MS Cha, CS Park, and SH Chung. Effect of electric fields on reattachment and propagation speed of tribrachial flames in laminar coflow jets. *Proceedings of the Combustion Institute*, 31(1):963–970, 2007.

[7] EN Volkov, AV Sepman, VN Kornilov, A Alexander Konnov, YS Shoshin, and LPH de Coey. Towards the mechanism of dc electric field effect on flat premixed flames. In *Proceedings of the European Combustion Meeting, Vienna, Austria*, volume 1417, 2009.

[8] Chao Li, Xiaomin Wu, Yiming Li, and Xuxing Wei. Experimental study of positive and negative dc electric fields in lean premixed spherically expanding flames. *Fuel*, 193:22–30, 2017.

[9] Hartwell F Calcote and Robert N Pease. Electrical properties of flames. burnerflames in longitudinal electric fields. *Industrial & Engineering Chemistry*, 43(12):2726–2731, 1951.

[10] Johannes Kuhl, Gordana Jovicic, Lars Zigan, and Alfred Leipertz. Transient electric field response of laminar premixed flames. *Proceedings of the Combustion Institute*, 34(2):3303–3310, 2013.

[11] Florian Altendorfner, Johannes Kuhl, Lars Zigan, and Alfred Leipertz. Study of the influence of electric fields on flames using planar lif and piv techniques. *Proceedings of the Combustion Institute*, 33(2):3195–3201, 2011.

[12] Johannes Kuhl, Thomas Seeger, Lars Zigan, Stefan Will, and Alfred Leipertz. On the effect of ionic wind on structure and temperature of laminar premixed flames influenced by electric fields. *Combustion and Flame*, 176:391–399, 2017.

[13] Dae Geun Park, Suk Ho Chung, and Min Suk Cha. Visualization of ionic wind in laminar jet flames. *Combustion and Flame*, 184:246–248, 2017.

[14] M Zake, I Barmina, and D Turlajs. Electric field control of polluting emissions from a propane flame. *Global Nest: the Int. J*, 3(2):95–108, 2001.

[15] A Sakhrieh, G Lins, F Dinkelacker, T Hammer, A Leipertz, and DW Branston. The influence of pressure on the control of premixed turbulent flames using an electric field. *Combustion and flame*, 143(3):313–322, 2005.

[16] EN Volkov, VN Kornilov, and LPH De Goey. Experimental evaluation of dc electric field effect on the thermoacoustic behaviour of flat premixed flames. *Proceedings of the Combustion Institute*, 34(1):955–962, 2013.

[17] Johannes Kuhl, Gordana Jovicic, Lars Zigan, Stefan Will, and Alfred Leipertz. Influence of electric fields on premixed laminar flames: Visualization of perturbations and potential for suppression of thermoacoustic oscillations. *Proceedings of the Combustion Institute*, 35(3):3521–3528, 2015.

[18] Sunny Karnani and Derek Dunn-Rankin. Detailed characterization of dc electric field effects on small non-premixed flames. *Combustion and Flame*, 162(7):2865–2872, 2015.

[19] Yang Zhang, Yuxin Wu, Hairui Yang, Hai Zhang, and Min Zhu. Effect of high-frequency alternating electric fields on the behavior and nitric oxide emission of laminar non-premixed flames. *Fuel*, 109:350–355, 2013.

[20] Teodoro Trindade. *Chemiluminescence spectral identity of premixed methane and propane flames*. UL. Instituto Superior Técnico, 2015.

[21] Jeffrey M Donbar, James F Driscoll, and Campbell D Carter. Reaction zone structure in turbulent nonpremixed jet flames—from ch-oh plif images. *Combustion and Flame*, 122(1-2):1–19, 2000.

[22] Jeongseog Oh and Dongsoon Noh. Laminar burning velocity of oxy-methane flames in atmospheric condition. *Energy*, 45(1):669–675, 2012.

[23] CK Law and CJ Sung. Structure, aerodynamics, and geometry of premixed flamelets. *Progress in Energy and Combustion Science*, 26(4-6):459–505, 2000.

[24] Stuart B Reed. Flame stretch—a connecting principle for blow-off data. *Combustion and Flame*, 11(3):177–189, 1967.

[25] Costa John Rallis and Ashton Martin Garforth. The determination of laminar burning velocity. *Progress in Energy and Combustion Science*, 6(4):303–329, 1980.